Published in final edited form as:

Precis Nanomed. 2018 October ; 1(3): 173–182. doi:10.33218/prnano1(3).181029.1.

Nanoparticle-Encapsulated Doxorubicin Demonstrates Superior Tumor Cell Kill in Triple Negative Breast Cancer Subtypes Intrinsically Resistant to Doxorubicin

Aimee E. Krausz[#1], **Brandon L. Adler**[#1], **Joy Makdisi**[1], **David Schairer**[1], **Jamie Rosen**[1], **Angelo Landriscina**[1], **Mahantesh Navati**[2], **Alan Alfieri**[2], **Joel M. Friedman**[2], **Joshua D. Nosanchuk**[3], **Alicia Rodriguez-Gabin**[4], **Kenny Q Ye**[5], **Hayley M. McDaid**[4,6,*], and **Adam J. Friedman**[1,2,7,*]

[1]Division of Dermatology, Department of Medicine, Albert Einstein College of Medicine, Bronx, New York, USA

[2]Department of Physiology and Biophysics, Albert Einstein College of Medicine, Bronx, New York, USA

[3]Department of Microbiology & Immunology, Albert Einstein College of Medicine, Bronx, New York, USA

[4]Department of Molecular Pharmacology, Albert Einstein College of Medicine, Bronx, New York, USA

[5]Department of Epidemiology and Population Health, Albert Einstein College of Medicine, Bronx, New York, USA

[6]Department of Medicine (Oncology), Albert Einstein College of Medicine, Bronx, New York, USA

[7]Department of Dermatology, George Washington School of Medicine, Washington, DC, USA

[#] These authors contributed equally to this work.

Abstract

The effect of size and release kinetics of doxorubicin-nanoparticles on anti-tumor efficacy was evaluated in a panel of human cancer cell lines, including triple-negative breast cancer (TNBC) cells that frequently demonstrate resistance to doxorubicin. Different nano-formulations of sol-gel-based Doxorubicin containing nanoparticles were synthesized. Increased cell kill in chemoreffactory triple-negative breast cancer cells was associated with the smallest size of nanoparticles and the slowest release of Dox. Modeling of dose-response parameters in Dox-sensitive versus Dox-resistant lines demonstrated increased E_{Max} and area under the curve in Dox-

[*]Corresponding Authors: Adam J. Friedman, MD. Department of Dennatology, George Washington School of Medicine and Health Sciences, 2150 Pennsylvania Avenue NW, Washington, DC 20037. Phone: 202-741-2600; ajfriedman@mfa.gwu.edu; Hayley McDaid, Ph.D. Department of Medicine (Oncology), Forchheimer 249B, 1300 Morris Park Avenue, Albert Einstein College of Medicine, Bronx, NY 10461. Phone: 718-430-8829; hayley.mcdaid@einstein.yu.edu.
[*]Co-senior authorship

Disclosures

A.J.F. and J.M.F. are co-inventors of the nanoparticle platform utilized in the studies described. This technology has been licensed to Zylo Therapeutics for commercial development.

resistant mesenchymal TNBC cells, implying potentially favorable activity in this molecular subtype of breast cancer. Mesenchymal TNBC cells demonstrated a high rate of fluorescent bead uptake suggestive of increased endocytosis, which may partially account for the enhanced efficacy of Dox-np in this subtype. Thus, manipulation of size and release kinetics of this nanoparticle platform is associated with enhanced dose-response metrics and tumor cell kill in therapeutically recalcitrant TNBC cell models. This platform is easily customizable and warrants further exploration.

Keywords

Experimental therapeutics; Nanoparticles; Triple-negative breast cancer; Doxorubicin; Drug resistance; Dose-response relationship

Purpose and Rationale

The purpose of this study was to synthesize and characterize a nanoparticle carrier for doxorubicin (Dox) and evaluate its biologic activity against a range of human cancer cell lines, focusing on TNBC in particular. Our goal was to investigate the pre-clinical anti-tumor activity of Dox-np relative to the parent drug.

Introduction

Doxorubicin, is a well-known anthracycline used primarily in combination chemotherapy for numerous malignancies, notably breast cancer, particularly triple-negative breast cancer (TNBC). The majority of TNBC patients receive a combination of taxane, doxorubicin and cyclophosphamide (TAC), as preoperative neoadjuvant chemotherapy, of which 25–45% achieve pathologic complete response (pCR) and have excellent long-term prognosis (1). Patients who fail TAC have poor prognosis with limited post-operative treatment options available (2). Response to TAC is predominately influenced by the molecular subtype of TNBC (3–5) of which mesenchymal (M) and BL2 tumors have the poorest response and long-term survival due to metastatic biology (2, 4), highlighting an unmet clinical need.

Encapsulation of Dox in a biocompatible nanoparticle platform could expand its narrow therapeutic index (6), enabling slow and sustained release of contents. This has the potential to limit toxicity since the theoretical maximum amount of drug is never in circulation at one time. The most well-known approach to nanoencapsulation of Dox is liposomal doxorubicin (Doxil®), FDA-approved in 1995 for Kaposi’s sarcoma. Despite proven clinical superiority and improved tolerability of liposomal doxorubicin, unique adverse events emerged with use (7). In an attempt to further refine Dox delivery, we utilized a sol-gel polymerization technique to create silane composite nanoparticles (8, 9). The platform was modified from a sol-gel-based protocol shown to successfully incorporate a range of therapeutic agents, including amphotericin (10) and sildenafil (11). These particles are formed from amorphous silicon oxide materials that polymerize into a highly structured porous lattice. The large surface area allows for greater drug loading as compared to liposomes (12), and the pore size distribution can be modified to alter the release rate of the encapsulated drug (13). Here we

describe their synthesis and enhanced anti-cancer activity, relative to Dox, in cancer cell lines.

Materials and Methods

Synthesis of Dox nanoparticles (Dox-np)

Clinical grade doxorubicin hydrochloride solution (2 mg/mL) was obtained from Pfizer (New York, NY). A hydrogel/glass composite incorporating Dox as the active component was produced as follows: Tetramethyl orthosilicate (TMOS) was hydrolyzed by adding HCl, followed by 20-minute sonication in an ice water bath. The mixture was refrigerated at 4°C until monophasic. Subsequently, different ratios of Tris-buffered saline and methanol were combined with chitosan, polyethylene glycol, doxorubicin (2 mg/mL), and TMOS-HCl to induce sample polymerization overnight at 4°C (see Table 1 for quantities).

The percent concentration of methanol utilized in Dox-np synthesis was 0%, 40%, 60%, and 80% (represented as Dox-np A0, A40, A60, A80). The hydrogel was subsequently lyophilized at ~200 mTorr for 48–72 hours and the resultant powder processed in a ball mill for ten 30-minute cycles to achieve smaller size and more uniform distribution. Control nanoparticles (control-np) were synthesized identically but without the incorporation of Dox.

(See Supplemental Information for additional methods.)

Results

Dox-np Diameter Characterization

Different variants of Dox-np were synthesized by changing the percent concentration of methanol in the gel phase (Table 1). However, once lyophilized, methanol was removed from the final product, abrogating potential cytotoxicity. The change in size of Dox-np as a function of initial methanol content was determined using dynamic light scattering. Imaging of Dox-np with a scanning electron microscope exhibited a distinct spherical structure with an irregular surface morphology, as shown in Figure 1A. The most significant differences were observed with the Dox-np (A0) and (A80), with an average diameter of 118.6 and 103.4 nm, respectively (Figure 1B).

Dox-np Release Profile

The amount of encapsulated Dox based on release in DMSO was calculated to be 14.5±0.35 ug/ml. The effect of temperature on the release profile of Dox-np was assessed by measuring the spectrophotometric absorbance of a Dox-np solution over time at both 4 and 37°C. Temperatures were selected to simulate storage and in vivo conditions, respectively.

At 4 °C, Dox-np (A0) immediately released 24.6% of encapsulated Dox in solution (t=0 hours) with no further release over 48 hours. In comparison, Dox-np (A80) initially released 11.9% with no further release over time (Figure 1C).

Increasing the temperature to 37°C prompted the continuous release of Dox from the porous matrix in a controlled manner (Figure 1D). The curve for both nano-formulations was characterized by an initial accelerated release from t=0 until t=6 hours, followed by a gradual increase until steady state was reached at 24 hours. Dox-np (A80) had a slower rate of release compared to Dox-np (A0), with lower maximum release after 48 hours. At t=0 hours, Dox-np (A0) released 37.5%, increasing to 60% at 6 hours and reaching a steady state by 24 hours of 68.3%. In comparison, at t=0 Dox-np (A80) released 17.2%, increasing to 31.7% at 6 hours and reaching a steady state by 24 hours of 44.1% release. Since, Dox-np (A80) had a slower release curve compared to Dox-np (A60) and (A40 – not shown). Future cell-based experiments focused mainly on A0 and A80.

Overall, the addition of methanol during Dox-np synthesis correlated with both decreased particle size, and slower initial and maximal release of encapsulated Dox, relative to Dox-np synthesized in the absence of methanol (A0)

Anti-Tumor Efficacy of Dox-np In Cells

We evaluated in-cell activity using multiparametric dose-response modeling in a panel of genetically diverse cancer cell lines. This approach generates metrics to facilitate robust comparison of Dox versus Dox-np using area under the curve (AUC), E_{Max} and EC_{50} as read outs of anti-cancer activity (14). Although EC_{50} is a commonly used metric of potency, it usually reflects a dose that suppresses proliferation. Dose-response curves for all cell lines indicated substantial variation between Dox, Dox-np (A0) and Dox-np (A80), as shown in Figure 2A.

High variation was observed for Dox such that curves dichotomized according to steep versus shallow slope, demarcating sensitive (S) and resistant (R) cohorts, respectively. This trend was also apparent for Dox-np (A0); however, Dox-np (A80) dose-response curves were steeper in the resistant cohort specifically, generating a more uniform dose-response relationship across all cell lines (Figure 2A). Dose-response parameters computed from sigmoidal dose-response curves are summarized in Table 2. Median values across all cell lines (black horizontal line) are depicted as box and whisker plots showing interquartile range (boxes) and variance (bars extending to 1.5× the interquartile range (Figure 2B). This analysis indicated increased AUC and E_{Max} for Dox-np (AO and A80) relative to Dox, although only E_{Max} reached statistical significance ($P < 0.05$; Wilcoxon signed rank test, Dox-np (A80) versus Dox). However, median EC_{50} increased for Dox-np, consistent with decreased sensitivity at doses associated with suppression of proliferation. Thus, improvements in dose-response parameters occurred at the high concentration range.

To facilitate a more nuanced evaluation of sensitive and resistant cohorts, dose-response parameters were recomputed for these 2 groups and box plots redrawn (Figure 2C). Resistant lines (SUM149PT, Hs578T and MDA-MB-157) were BL2 and mesenchymal (M) subtypes of TNBC that represent types of disease with aggressive, metastatic tumor biology (15). Dox-np (A80) had statistically significantly increased E_{Max} relative to Dox in the resistant cohort ($P < 0.001$; Wilcoxon signed rank test) and slightly increased AUC and decreased EC_{50}, consistent with improved anti-tumor activity overall. In the sensitive cohort, Dox had comparable EC_{Max} as Dox-np, while AUC and EC_{50} values showed decreased

effect of Dox-np relative to Dox. This lack of sensitization by Dox-np in sensitive cohorts is also shown in dose-response curves for individual cell lines (Figure S1). Thus, Dox-np has superior efficacy specifically in BL2 and M subtypes of TNBC in vitro.

Dox-np Has Superior Tumor Cell Kill in BL2 and M Subtypes of Breast Cancer

High-dose Dox-np (A80) caused enhanced tumor cell kill in chemoresistant TNBC cell lines (Figure 3). Dox was unable to elicit the same degree of tumor cell kill at equivalent concentrations (800nM). At lower doses (100nM), the difference in survival between Dox and Dox-np was not remarkable, consistent with other data indicating that the superiority of Dox-np is limited to high concentrations.

Increased Endocytosis as a Mechanism for Superior Efficacy of Dox-np

Nanoparticles are thought to be taken into cells via endocytosis (16), although understanding nanoparticle uptake remains a challenge in the field. To address differences in uptake between TNBC subtypes, we used fluorescent beads as a surrogate to monitor Dox-np uptake. Both M type cell lines (Hs578T and MDA-MB-157) incorporated significantly more beads than BL1 and unclassified (UN) subtypes (Table 3 and Figure S2), implying increased endocytosis in Dox-refractory M type TNBC cells. This associates with the superior E_{Max} and high rate of cell death by Dox-np in these cells and could offer mechanistic insight for future studies.

Discussion and Conclusion

The need to develop and test therapies with superior therapeutic index is a driving force in modern cancer drug development as we advance toward treating cancer as a chronic condition. An exciting advance is the development of nanoparticle technology, exemplified by the clinical success of Doxil and Abraxane. The enthusiasm surrounding nanotechnology centers on the potential to modulate pharmacokinetics to enhance drug delivery and pharmacodynamics, while reducing systemic toxicity. We synthesized a malleable nanoparticle capable of releasing Dox in a time- and dose-regulated manner. A major benefit of nanotechnology such as ours is the ability to customize various elements involved in synthesis, in this case, manipulating initial methanol content, which significantly affected performance parameters including size and release rate and correlated with improved in vitro activity.

Tris-buffered saline possesses amines that block silanol interactions between nanoparticles thereby inhibiting aggregation, which would otherwise impair the EPR effect and diminish ability to accumulate in tumor tissue. Enhanced reduction of individual particle size was achieved by choosing TMOS and methanol as the alkoxide and alcohol, respectively, as each contributes independently to minimization of size (17). Polyethylene glycol (PEG) was incorporated into the body of the nanoparticle as it has been demonstrated that PEG controls the pore size in the sol-gel matrix of our platform and thus is the primary effector of release characteristics (12, 18). As a steric stabilizer, PEG also contributes to maintaining small individual particle size by interfering with inter-particle hydrogen bonding to decrease nanoparticle aggregation (19).

Supplementary Material

Refer to Web version on PubMed Central for supplementary material.

Acknowledgments

This work was supported by National Cancer Institute Grant CA077263 and the Breast Cancer Research Foundation. A.J.F. would like to acknowledge the Dermatology Foundation Career Development Awards Program.

Abbreviations:

pCR	Pathologic Complete Response
TNBC	Triple-Negative Breast Cancer
AUC	Area under the curve
Dox	Doxorubicin
Dox-np	Doxorubicin-Nanoparticles

References

1. Gonzalez-Angulo AM, McGuire SE, Buchholz TA, Tucker SL, Kuerer HM, Rouzier R, et al. Factors predictive of distant metastases in patients with breast cancer who have a pathologic complete response after neoadjuvant chemotherapy. Journal of clinical oncology : official journal of the American Society of Clinical Oncology. 2005;23(28):7098–104. Epub 2005/09/30. doi: 10.1200/JCO.2005.11.124. PubMed . [PubMed: 16192593]
2. Liedtke C, Mazouni C, Hess KR, Andre F, Tordai A, Mejia JA, et al. Response to neoadjuvant therapy and long-term survival in patients with triple-negative breast cancer. Journal of clinical oncology : official journal of the American Society of Clinical Oncology. 2008;26(8):1275–81. Epub 2008/02/06. doi: 10.1200/JCO.2007.14.4147. PubMed . [PubMed: 18250347]
3. Prat A, Parker JS, Karginova O, Fan C, Livasy C, Herschkowitz JI, et al. Phenotypic and molecular characterization of the claudin-low intrinsic subtype of breast cancer. Breast cancer research: BCR. 2010;12(5):R68 Epub 2010/09/04. doi: 10.1186/bcr2635. PubMed ; PubMed Central PMCID: PMC3096954. [PubMed: 20813035]
4. Masuda H, Baggerly KA, Wang Y, Zhang Y, Gonzalez-Angulo AM, Meric-Bernstam F, et al. Differential response to neoadjuvant chemotherapy among 7 triple-negative breast cancer molecular subtypes. Clinical cancer research : an official journal of the American Association for Cancer Research. 2013;19(19):5533–40. Epub 2013/08/21. doi: 10.1158/1078-0432.CCR-13-0799. PubMed ; PubMed Central PMCID: PMC3813597. [PubMed: 23948975]
5. Lehmann BD, Jovanović B, Chen X, Estrada MV, Johnson KN, Shyr Y, et al. Refinement of Triple-Negative Breast Cancer Molecular Subtypes: Implications for Neoadjuvant Chemotherapy Selection. PLoS ONE. 2016;11(6):e0157368. doi: 10.1371/journal.pone.0157368. [PubMed: 27310713]
6. Gref R, Minamitake Y, Peracchia MT, Trubetskoy V, Torchilin V, Langer R. Biodegradable long-circulating polymeric nanospheres. Science. 1994;263(5153):1600–3. Epub 1994/03/18. PubMed . [PubMed: 8128245]
7. Barenholz Y Doxil(R)--the first FDA-approved nano-drug: lessons learned. Journal of controlled release : official journal of the Controlled Release Society. 2012;160(2):117–34. Epub 2012/04/10. doi: 10.1016/j.jconrel.2012.03.020. PubMed . [PubMed: 22484195]
8. Friedman AJ, Han G, Navati MS, Chacko M, Gunther L, Alfieri A, et al. Sustained release nitric oxide releasing nanoparticles: characterization of a novel delivery platform based on nitrite containing hydrogel/glass composites. Nitric oxide : biology and chemistry / official journal of the

Nitric Oxide Society. 2008;19(1):12–20. Epub 2008/05/07. doi: 10.1016/j.niox.2008.04.003. PubMed .

9. Gupta R, Kumar A. Bioactive materials for biomedical applications using sol-gel technology. Biomed Mater. 2008;3(3):034005 Epub 2008/08/12. doi: 10.1088/1748-6041/3/3/034005. PubMed . [PubMed: 18689920]
10. Sanchez DA, Schairer D, Tuckman-Vernon C, Chouake J, Kutner A, Makdisi J, et al. Amphotericin B releasing nanoparticle topical treatment of Candida spp. in the setting of a burn wound. Nanomedicine : nanotechnology, biology, and medicine. 2014;10(1):269–77. Epub 2013/06/19. doi: 10.1016/j.nano.2013.06.002. PubMed .
11. Han G, Tar M, Kuppam DS, Friedman A, Melman A, Friedman J, et al. Nanoparticles as a novel delivery vehicle for therapeutics targeting erectile dysfunction. The journal of sexual medicine. 2010;7(1 Pt 1):224–33. Epub 2009/09/22. doi: 10.1111/j.1743-6109.2009.01507.x. PubMed ; PubMed Central PMCID: PMC2864537.
12. Seleem MN, Munusamy P, Ranjan A, Alqublan H, Pickrell G, Sriranganathan N. Silica-antibiotic hybrid nanoparticles for targeting intracellular pathogens. Antimicrobial agents and chemotherapy. 2009;53(10):4270–4. Epub 2009/08/12. doi: 10.1128/AAC.00815-09. PubMed ; PubMed Central PMCID: PMC2764215. [PubMed: 19667284]
13. Yuan H, Bao X, Du YZ, You J, Hu FQ. Preparation and evaluation of SiO2-deposited stearic acid-g-chitosan nanoparticles for doxorubicin delivery. International journal of nanomedicine. 2012;7:5119–28. Epub 2012/10/12. doi: 10.2147/IJN.S35575. PubMed ; PubMed Central PMCID: PMC3463401. [PubMed: 23055724]
14. Fallahi-Sichani M, Honarnejad S, Heiser LM, Gray JW, Sorger PK. Metrics other than potency reveal systematic variation in responses to cancer drugs. Nat Chem Biol. 2013;9(11):708–14. doi: 10.1038/nchembio.1337. PubMed ; PubMed Central PMCID: PMCPMC3947796. [PubMed: 24013279]
15. Lehmann BD, Bauer JA, Chen X, Sanders ME, Chakravarthy AB, Shyr Y, et al. Identification of human triple-negative breast cancer subtypes and preclinical models for selection of targeted therapies. The Journal of clinical investigation. 2011;121(7):2750–67. Epub 2011/06/03. doi: 10.1172/JCI45014. PubMed ; PubMed Central PMCID: PMC3127435. [PubMed: 21633166]
16. Moore A, Weissleder R, Bogdanov A Jr. Uptake of dextran-coated monocrystalline iron oxides in tumor cells and macrophages. Journal of magnetic resonance imaging : JMRI. 1997;7(6):1140–5. Epub 1997/12/24. PubMed . [PubMed: 9400860]
17. Stöber W Controlled growth of monodisperse silica spheres in the micron size range. J Colloid Interface Sci. 1968;26(1):62–9. doi: 10.1016/0021-9797(68)90272-5.
18. Han G, Friedman A, Friedman J. Nitric Oxide Releasing Nanoparticle Synthesis and Characterization In: McCarthy HO, Coulter JA, editors. Nitric oxide : biology and chemistry / official journal of the Nitric Oxide Society. Methods in Molecular Biology. 704: Humana Press; 2011 p. 187–95.
19. Xu H, Yan F, Monson EE, Kopelman R. Room-temperature preparation and characterization of poly (ethylene glycol)-coated silica nanoparticles for biomedical applications. Journal of Biomedical Materials Research Part A. 2003;66A(4):870–9. doi: 10.1002/jbm.a.10057.
20. Kirtane AR, Kalscheuer SM, Panyam J. Exploiting nanotechnology to overcome tumor drug resistance: Challenges and opportunities. Advanced drug delivery reviews. 2013;65(13–14):1731–47. Epub 2013/09/17. doi: 10.1016/j.addr.2013.09.001. PubMed ; PubMed Central PMCID: PMC3849460. [PubMed: 24036273]
21. El Andaloussi S, Mager I, Breakefield XO, Wood MJA. Extracellular vesicles: biology and emerging therapeutic opportunities. Nat Rev Drug Discov. 2013;12(5):347–57. doi: 10.1038/nrd3978. [PubMed: 23584393]

The cellular mechanism that results in improved anti-tumor efficacy of nanoparticle formulations of cytotoxic drugs relative to free drug is multifactorial and includes enhanced permeation and retention (EPR) effects highly dependent on tumor microenvironment, increased uptake into cells via endocytosis, and circumvention of drug transporter activation / recruitment, such as ABC family transporters including Pgp (20, 21). The most impressive anti-tumor property of Dox-np is the potent cell-kill ability in refractory TNBC cell lines representative of disease with unmet clinical need. Thus, these are translationally significant findings that warrant future in vivo evaluation of Dox-np.

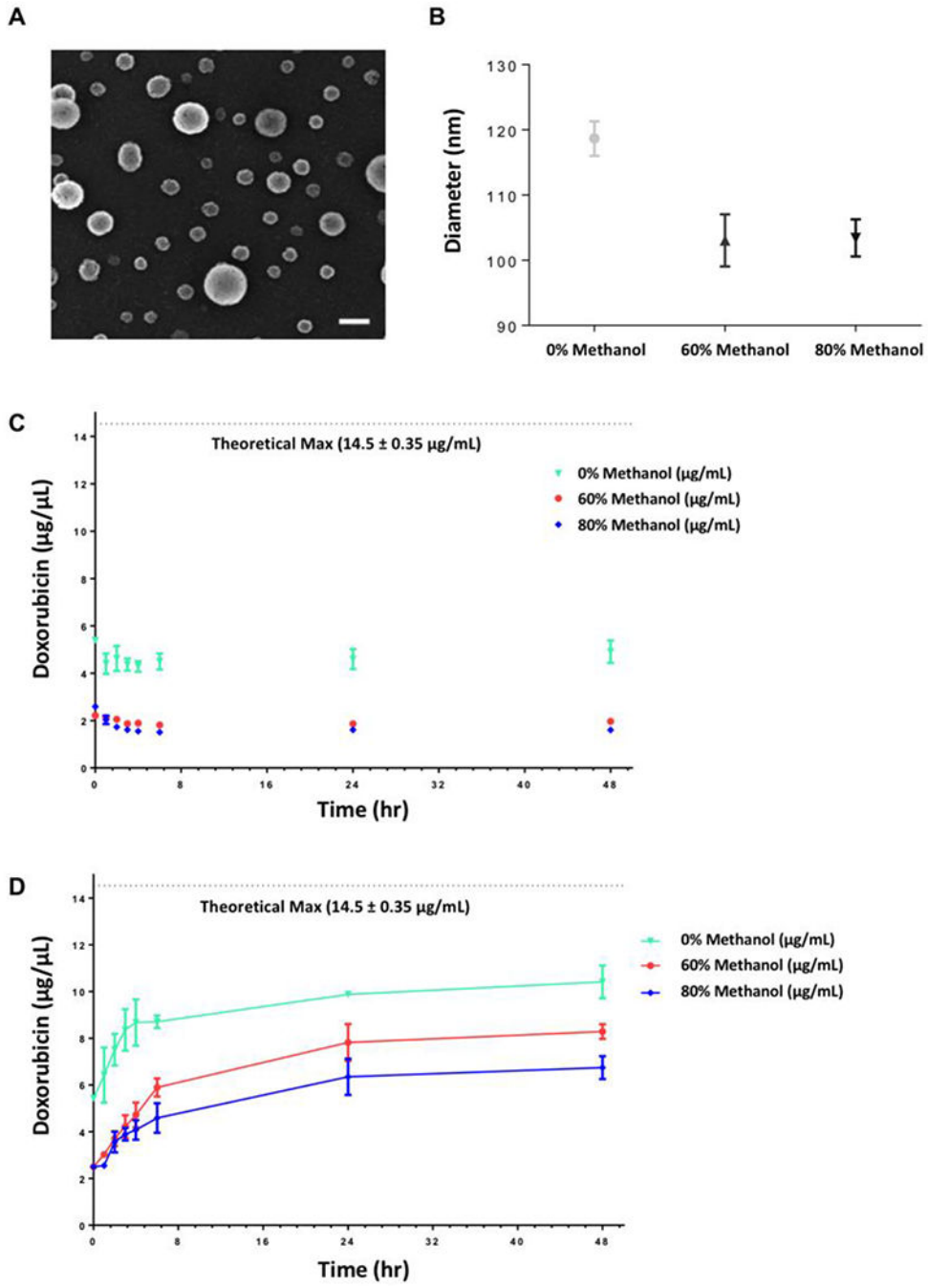

Figure 1.

Characterization of Dox-np Size and Effect of Temperature on Doxorubicin Release. (A) Representative scanning electron microscopy images of Dox-np particles. (B) Hydrodynamic diameter of nanoparticles assessed via dynamic light scattering revealed decreasing nanoparticle size with increasing methanol content. Scale bar = 200 nm, n=2. (C) At 4°C, minimal Dox was released in an initial burst at t = 0 hours with no further release over 48 hours. (D) At 37°C, Dox was released from the nanoparticle matrix with an acceleration from t=0–6 hours, followed by a gradual increase until steady state at 24 hours.

Dox-np (A80) had a slower rate of release compared to Dox-np (A0), with lower maximum release after 48 hours. As depicted, theoretical maximum release was never achieved. Error bars denote χ ± sem. n=2.

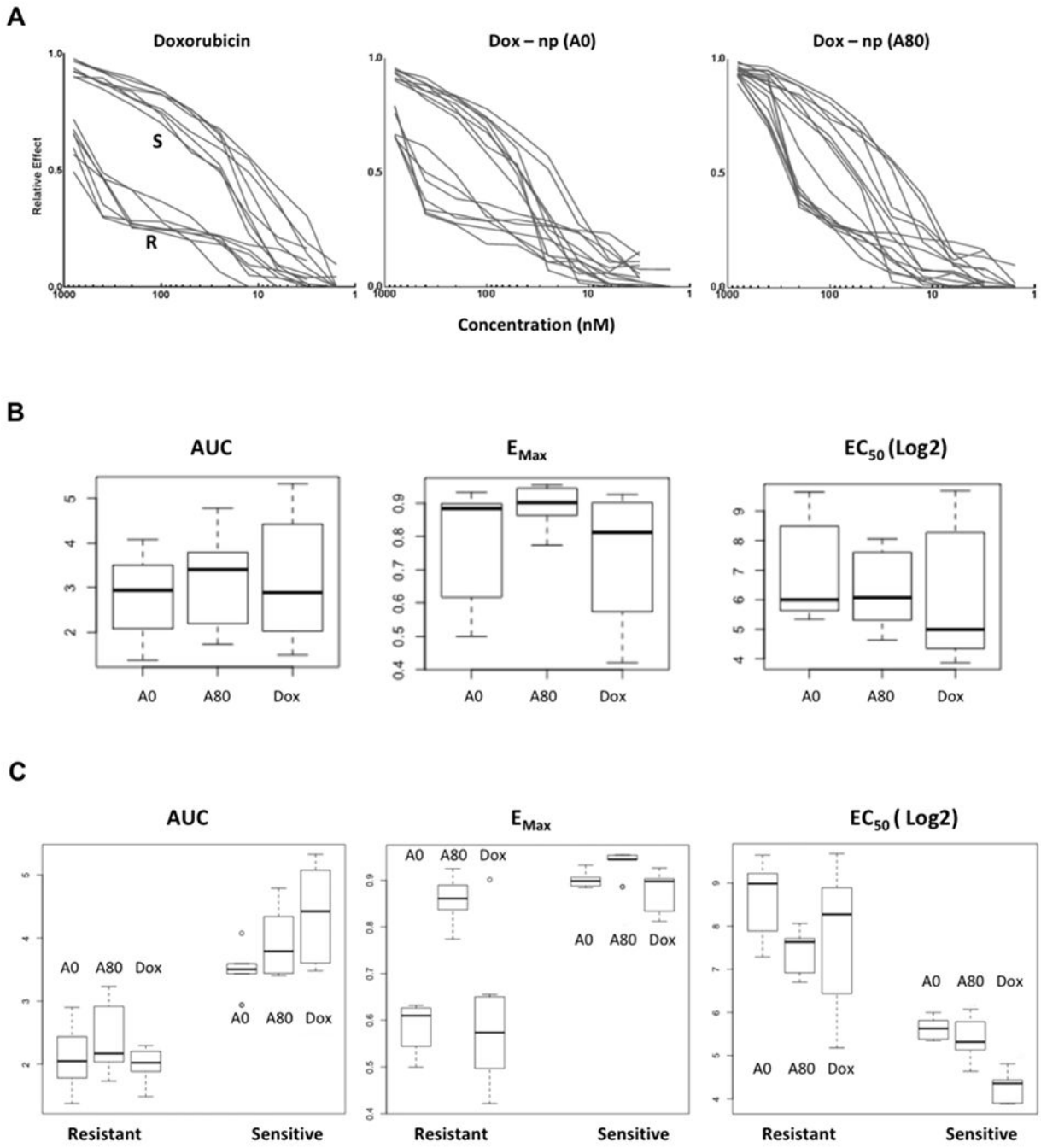

Figure 2.

Improved Dose-Response Relationship of Dox-np versus Doxorubicin In Triple-Negative Breast Cancer (TNBC). (A) Dose-response curves representing different variation in dose-response relationships. Patterns of dose-response are shown for Dox, Dox-np (A0) and Dox-np (A80). Each curve represents a dataset for one cell line. High variation was observed for doxorubicin and curves separate into 2 cohorts representing sensitive (S) and resistant (R) lines. This separation was also evident for Dox-np (A0). Dox-np (A80) gave a more uniform distribution. (B) Distribution of dose-response parameters AUC, E_{Max} and EC_{50} for Dox-np

*(A80) relative to Dox, or Dox-np (A0) across 6 cancer cell lines. Values were computed from sigmoidal dose-response simulations and drawn as box and whisker plots showing median value (black horizontal line) with interquartile range (boxes). Bars extending to 1.5× the interquartile range indicate variance. Among all cell lines, E_{Max} is most improved relative to Dox. (C) Distribution of dose-response parameters segregated according to Dox resistance or sensitivity. Resistant lines were mesenchymal TNBC's (BL2 and M subtype). Dox-np (A80) had statistically significantly superior E_{Max} relative to Dox in the resistant cohort (*P *< 0.0001; Wilcoxon signed rank test) with slightly increased AUC (*P*=NS*) and statistically significantly decreased EC_{50} (*P *< 0.005; Wilcoxon signed rank test), consistent with improved anticancer activity overall. Outliers are shown as non-connected data points in the plots.*

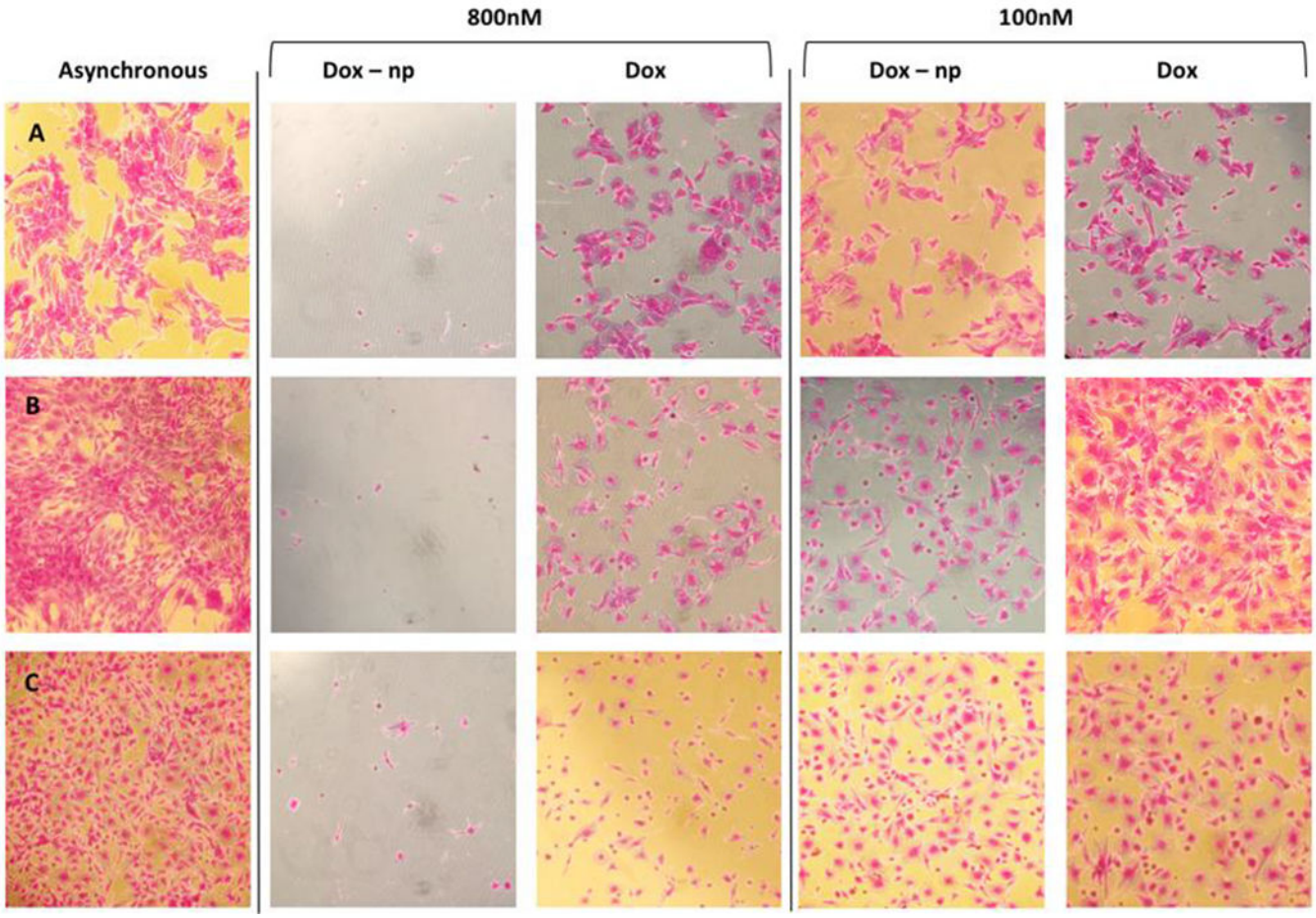

Figure 3.

E_{Max} Doses of Dox-np Cause Enhanced Cell Death Relative to Doxorubicin in Chemorefractory Triple-Negative Breast Cancer (TNBC). Surviving TNBC cells in (A) SUM149PT, (B) Hs578T, and (C) MDA-MB-157 following incubation with either Dox-np (A80) or Dox. Representative images were obtained from SRB-stained plates, as described in Materials and Methods (10× magnification).

Table 1:

Dox-np Synthesized with Varying Concentrations of methanol

0% MeOH nanoparticles	40% MeOH nanoparticles	60% MeOH nanoparticles	80% MeOH nanoparticles	100% MeOH nanoparticles
22 mL Tris (50mM)	12.4 mL Tris (50mM)	7.6 mL Tris (50mM)	2.8 mL Tris (50mM)	24 mL methanol
1.5 mL chitosan (5mg/ml)	9.6 mL methanol	14.4 mL methanol	19.2 mL methanol	1.5 mL chitosan
1.5 ml PEG 400	1.5 ml chitosan	1.5 ml chitosan	1.5 ml chitosan	1.5 ml PEG 400
2 mL adriamycin (2mg/ml)	1.5 mL PEG 400	1.5 mL PEG 400	1.5 mL PEG 400	2 mL adriamycin (2mg/ml)
3 mL TMOS	2 mL adriamycin (2mg/mL)	2 mL adriamycin (2mg/mL)	2 mL adriamycin (2mg/mL)	3 mL TMOS
0.6 mL HCl (1mM)	3 mL TMOS	3 mL TMOS	3 mL TMOS	0.6 mL HCl (1mM)
	0.6 mL HCl (1mM)	0.6 mL HCl	0.6 mL HCl (1mM)	

In the polymenzation phase, the percent concentration of methanol was increased between different samples. 0%, 40%, 60%, 80% and 100% methanol content correspond to Dox-np (A0), (A40), (A60), (A80), and (A100), respectively. See methods for additional detail.

Table 2:

Dose-Response Parameters for Dox versus Dox-np in a Panel of Cancer Cell Lines

		E_{Max}		AUC		EC_{50} (Log_2)	
Tumor Type	***Cell Line***	**Dox**	**Dox-np (A80)**	**Dox**	**Dox-np (A80)**	**Dox**	**Dox-np (A80)**
TNBC-BL2	**Suml49PT**	0.52	0.88	1.99	2.41	5.93	7.36
TNBC-M	**Hs578T**	0.68	0.88	2.01	2.11	8.45	7.66
TNBC-M	**MDA-MB-157**	0.50	0.80	1.92	3.02	9.63	6.92
TNBC-BL1	**MDA-MB-468**	0.89	0.95	5.07	4.33	3.89	5.13
NSCLC	**A549**	0.90	0.95	5.26	5.04	3.42	4.34
Ovarian	**HEY**	0.87	0.93	4.21	3.85	4.37	5.45

Dose-Response modeling enabled computation of metrics across 6 cancer cell lines, including E_{max} (a measure of efficacy), AUC (area under the dose-response curve) and EC_{50} (a measure of potency). Cell lines highlighted in grey represent the resistant cohort and are molecular subtypes of TNBC that are metastatic and have poor overall survival. Dox-np (A80) demonstrated dramatically superior E_{Max} in these cell lines, relative to Dox.

TNBC – Triple negative breast cancer; BL1 – Basal-like 1; BL2 – Basal-like 2; M – Mesenchymal; NSCLC – Non-small cell lung carcinoma.

Table 3:

Increased Fluorescent Bead Uptake in Mesenchymal Versus Basal TNBC

Histology / Subtype	Cell Line	% Fluorescent Bead Uptake * (Number of beads per cell - range)
BL1	MDA-MB-468	2.5 (1–3)
UN	BT-20	1.5% (1–2)
M	Hs578T	90% (1–15)
M	MDA-MB-157	43% (1–6)

* Bead uptake was quantified by counting 6 fields at 40× magnification and determining die number of cells with red fluorescence as a proportion of the total number of cells (counted by phase). The range of spots per cell are indicated in parentheses. BL1 = basal-like 1; M = mesenchymal; TNBC = triple-negative breast cancer; UN = unclassified.